J|A|C|S ARTICLES

Published on Web 08/03/2010

Organic Single-Crystalline p−n Junction Nanoribbons

Yajie Zhang,[†] Huanli Dong,[†] Qingxin Tang,[†] Sunzida Ferdous,[‡] Feng Liu,[‡] Stefan C. B. Mannsfeld,[§] Wenping Hu,*[,†] and Alejandro L. Briseno*[,‡]

Beijing National Laboratory for Molecular Sciences, Key Laboratory of Organic Solids, Institute of Chemistry, Chinese Academy of Sciences, Beijing 100190, China, Polymer Science and Engineering, University of Massachusetts, Amherst, Massachusetts 01003, and Stanford Synchrotron Radiation Lightsource, Menlo Park, California 94025

Received April 11, 2010; E-mail: huwp@iccas.ac.cn; abriseno@mail.pse.umass.edu

Abstract: This article focuses on the growth and transport properties of organic single-crystalline p−n junction nanoribbons. The development of organic nanoelectronics requires the fabrication of organic nanometer-sized p−n junctions for high-performance devices and integrated circuits. Here we demonstrate the formation of single-crystalline p−n junction nanoribbons of organic semiconductors by selective crystallization of copper hexadecafluorophthalocyanine (F_{16}CuPc, n-type) on copper phthalocyanine (CuPc, p-type) single-crystalline nanoribbons. The crystallization of F_{16}CuPc onto CuPc requires several parameters, including similar molecular structures, similar lattice constants, and π-stacking along the nanoribbon axis. Ambipolar transport of the p−n junction nanoribbons was observed in field-effect transistors with balanced carrier mobilities of 0.05 and 0.07 $cm^2\ V^{-1}\ s^{-1}$ for F_{16}CuPc and CuPc, respectively. A basic p−n junction nanoribbon photovoltaic device showed current rectification under AM 1.5 simulated light. The discrete p−n junction nanoribbons may serve as ideal systems for understanding basic charge-transport and photovoltaic behaviors at organic−organic interfaces.

Introduction

p−n junctions are of great importance in modern electronics, as they are the most basic elements for devices and circuits and serve as good model systems for the understanding of semiconductors and nanostructures.[1] With the rapid advancement of nanoelectronics, one-dimensional (1D) p−n junctions have attracted particular attention because of their optoelectronic properties as well as their use as building blocks for highly sophisticated nanodevices. For example, cross-wire p−n junctions assembled from inorganic nanowires demonstrate excellent rectification and light-emitting behavior.[2] Coaxial p−n or p−i−n nanowires have also been employed in optoelectronic applications,[3] such as nanowire photovoltaic devices.[3c] Organic−inorganic hybrid p−n nanostructures have also been recently utilized to demonstrate photovoltaic behavior.[4] These novel concepts and interesting properties of nanometer-sized p−n junctions offer great opportunities in both fundamental research and practical applications.

Despite the encouraging progress on inorganic and hybrid p−n junction nanostructures, few reports have addressed p−n junctions on pure organic single-crystalline semiconductors. One reason is the difficulty of fabricating organic p−n junctions. For instance, the techniques for the fabrication of inorganic p−n junctions, such as oxidation, diffusion of dopants, and ion implantation, are inapplicable to organic semiconductors.[1,5] Moreover, it is challenging to choose the proper complementary materials for fabricating p−n single-crystalline junctions. In this paper, we focus on the synthesis of organic p−n junction nanoribbons consisting of single-crystalline bilayers of copper phthalocyanine (CuPc) and copper hexadecafluorophthalocyanine (F_{16}CuPc). Polycrystalline p−n junctions of these two compounds and their photovoltaic behaviors have already been well-documented.[6] The junction structure, electronic states, and interfacial charge transfer have also been studied, even at the molecular level.[6] Although a great deal of work on polycrystalline thin-film junctions has been published, the long-range disorder has been detrimental to device performance, and such a morphology does not reflect the intrinsic performance of organic heterojunctions. On the other

[†] Chinese Academy of Sciences.
[‡] University of Massachusetts.
[§] Stanford Synchrotron Radiation Lightsource.

(1) Sze, S. M. *Physics of Semiconductor Devices*, 2nd ed.; Wiley: New York, 1981.
(2) (a) Duan, X.; Huang, Y.; Cui, Y.; Wang, J.; Lieber, C. M. *Nature* **2001**, *409*, 66–69. (b) Huang, Y.; Duan, X.; Lieber, C. M. *Small* **2005**, *1*, 142–147.
(3) (a) Garnett, E. C.; Yang, P. *J. Am. Chem. Soc.* **2008**, *130*, 9224–9225. (b) Hwang, Y. J.; Boukai, A.; Yang, P. *Nano Lett.* **2009**, *9*, 410–415. (c) Dong, Y.; Tian, B.; Kempa, T.; Lieber, C. M. *Nano Lett.* **2009**, *9*, 2183–2187.
(4) (a) Guo, Y.; Tang, Q.; Liu, H.; Zhang, Y.; Li, Y.; Hu, W.; Wang, S.; Zhu, D. *J. Am. Chem. Soc.* **2008**, *130*, 9198–9199. (b) Guo, Y.; Zhang, Y.; Liu, H.; Lai, S.; Li, Y.; Li, Y.; Hu, W.; Wang, S.; Che, C.; Zhu, D. *J. Phys. Chem. Lett.* **2010**, *1*, 327–330. (c) Briseno, A. L.; Holcombe, T. W.; Boukai, A. I.; Garnett, E. C.; Shelton, S. W.; Fréchet, J. M. J.; Yang, P. *Nano Lett.* **2010**, *10*, 334–340.
(5) (a) Wu, Y.; Fan, R.; Yang, P. *Nano Lett.* **2002**, *2*, 83–86. (b) Gudiksen, M. S.; Lauhon, L. J.; Wang, J.; Smith, D. C.; Lieber, C. M. *Nature* **2002**, *415*, 617–620. (c) Caroff, P.; Dick, K. A.; Johansson, J.; Messing, M. E.; Deppert, K.; Samuelson, L. *Nat. Nanotechnol.* **2009**, *4*, 50–55.
(6) (a) Huang, Y.; Li, H.; Ma, J.; Huang, H.; Chen, W.; Wee, A. T. S. *Langmuir* **2010**, *26*, 3329–3334. (b) Ye, R.; Baba, M.; Suzuki, K.; Mori, K. *Appl. Surf. Sci.* **2008**, *254*, 7885–7888. (c) Videlot-Ackermann, C.; Ackermann, J.; Fages, F. *Synth. Met.* **2007**, *157*, 551–557. (d) Lau, K. M.; Tang, J. X.; Sun, H. Y.; Lee, C. S.; Lee, S. T.; Yan, D. *Appl. Phys. Lett.* **2006**, *88*, 173513.

 10.1021/ja102779x

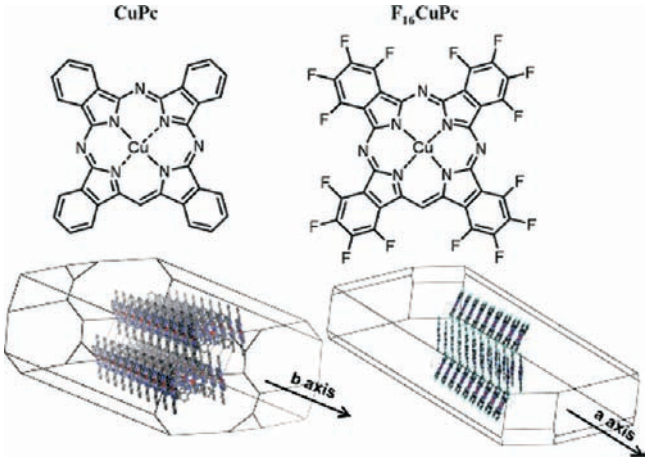

Figure 1. Chemical structures of CuPc and F_{16}CuPc and solid-state packing of these molecules in the 1D nanoribbons. The theoretically predicted crystal habit [Bravais−Friedel−Donnay−Harker (BFDH) method] exhibits an elongation along the [010] and [100] directions for CuPc and F_{16}CuPc, respectively. The predicted crystal habit is in agreement with the nanowire morphology observed in diffraction measurements. The BFDH crystal habit was constructed using Mercury software (http://www.ccdc.cam.ac.uk/mercury).

hand, the formation of organic single-crystal p−n heterojunctions, especially 1D single-crystal nanostructures, is still a great challenge in the area of organic electronics, and no successful case has been realized to date. Here we report the fabrication of organic single-crystal p−n junction nanoribbons of CuPc and F_{16}CuPc and demonstrate their use in ambipolar transistors and discrete nanoribbon solar cells. The single-crystalline p−n junctions form as a result of interfacial matching parameters such as growth along a face with strong attractive interactions (e.g., along the $\pi-\pi$ stacking direction) and similar lattice constants (for epitaxial growth) at interfaces of the two respective crystal faces.[7,8] One might expect that the organic single-crystalline p−n junction device architecture can serve as a potential tool for fundamental studies such as investigations of interfacial charge-transport phenomena.

The materials selected for use in producing the p−n junction nanoribbons were metal phthalocyanines, a class of planar, 2D aromatic molecules with excellent optoelectronic properties. Among them, CuPc (Figure 1) has attracted much attention as a p-type organic semiconductor with high thermal/chemical stability and excellent field-effect mobilities (up to 1.0 $cm^2\ V^{-1}\ s^{-1}$).[9] Single-crystalline nanoribbons of CuPc were grown using the physical vapor transport (PVT) technique. F_{16}CuPc, the fluorinated analogue of CuPc (Figure 1), adopts a similar packing motif and is known as an air stable, n-type organic semiconductor.[10] Electron mobilities of $\sim$0.6 $cm^2\ V^{-1}s^{-1}$ for the n-type organic semiconductor have been reported.[10c] Single-crystalline nanoribbons of F_{16}CuPc were also grown using PVT. The single-crystal lattice parameters of CuPc and F_{16}CuPc[11] are $a = 14.628$ Å, $b = 4.790$ Å, $c = 19.407$ Å, $\alpha = 90.00°$, $\beta = 120.93°$, $\gamma = 90.00°$ and $a = 4.796$ Å, $b = 10.228$ Å, $c = 28.002$ Å, $\alpha = 86.41°$, $\beta = 87.89°$, $\gamma = 81.39°$, respectively. Powder X-ray diffraction (XRD) and electron diffraction data (discussed below) corroborated that the CuPc and F_{16}CuPc nanoribbon structures are the same as the respective single-crystal structures. In the nanoribbons, the molecules of CuPc are stacked along the *b* axis (i.e., in the [010] direction; Figure 1) whereas the F_{16}CuPc molecules are stacked along the *a* axis (i.e., in the [100] direction; Figure 1). There is only a negligible (0.13%) mismatch between the lattice parameters of F_{16}CuPc ($a = 4.796$ Å) and CuPc ($b = 4.790$ Å) along the $\pi-\pi$ stacking direction of the nanoribbons, which is important for epitaxial crystallization of F_{16}CuPc on CuPc.

Experimental Section

The synthesis of the p−n junction nanoribbons was performed using the PVT technique in a two-zone horizontal tube furnace.[12] Single-crystalline nanoribbons of CuPc were first grown on Si/SiO_2 substrates. The CuPc nanoribbons were then used as the templates for selective crystallization of F_{16}CuPc. Scanning electron microscopy (SEM) images were obtained with a Hitachi S-4300SE scanning electron microscope, and transmission electron microscopy (TEM) results were carried out with a JEOL 2010 transmission electron microscope. Optical images were captured with a Leica DM 400M microscope. Atomic force microscopy (AFM) was performed with a Nanoscopy IIIa atomic force microscope. The structures were analyzed by powder XRD (Rigaku D/max 2500). Micro-Raman spectroscopy on the samples was performed in the backscattering geometry using a Renishaw InVia system with a 514.5 nm argon ion laser. Transistor characteristics were recorded with a Keithley 4200 SCS and a Micromanipulator 6150 probe station in a clean and shielded box at room temperature. Photovoltaic measurements were carried out using a Janis probe station equipped with a solar simulator (Oriel).

Results and Discussion

CuPc nanoribbons predeposited on substrates are shown in Figure 2a,b. The width of the nanoribbons ranged from several tens to several hundred nanometers and the lengths from 20 to 50 μm. The substrates with CuPc nanoribbons were subsequently used as templates for the crystallization of F_{16}CuPc. Figure 2c,d shows SEM and dark-field microscope images of the p−n junction nanoribbons that clearly indicate the selective growth of F_{16}CuPc on CuPc templates. An attractive feature of this system is the ability to easily generate p−n junction nanoribbons in large quantities (Figure 2e). The formation of organic p−n junction nanoribbons in large quantities and, if possible, over

(7) (a) Chen, W.; Huang, H.; Chen, S.; Gao, X.; Wee, A. T. S. *J. Phys. Chem. C* **2008**, *112*, 5036–5042. (b) Chen, W.; Huang, H.; Chen, S.; Huang, Y.; Wee, A. T. S. *Chem. Mater.* **2008**, *20*, 7017–7021. (c) Chen, W.; Chen, S.; Chen, S.; Huang, Y.; Huang, H.; Qi, D.; Gao, X.; Ma, J.; Wee, A. T. S. *J. Appl. Phys.* **2009**, *106*, 064910.
(8) (a) Zhu, F.; Lou, K.; Huang, L.; Yang, J.; Zhang, J.; Wang, H.; Geng, Y.; Yan, D. *Appl. Phys. Lett.* **2009**, *95*, 203106. (b) Wang, H.; Zhu, F.; Yang, J.; Geng, Y.; Yan, D. *Adv. Mater.* **2007**, *19*, 2168–2171. (c) Zhu, F.; Wang, H.; Song, D.; Lou, K.; Yan, D. *Appl. Phys. Lett.* **2008**, *93*, 103308. (d) Zhu, F.; Yang, J.; Song, D.; Li, C.; Yan, D. *Appl. Phys. Lett.* **2009**, *94*, 143305.
(9) (a) Bao, Z.; Lovinger, A. J.; Dodabalapur, A. *Appl. Phys. Lett.* **1996**, *69*, 3066–3068. (b) Zeis, R.; Siegrist, T.; Kloc, C. *Appl. Phys. Lett.* **2005**, *86*, 022103. (c) Tang, Q.; Li, H.; He, M.; Hu, W.; Liu, C.; Chen, K.; Wang, C.; Liu, Y.; Zhu, D. *Adv. Mater.* **2006**, *18*, 65–68. (d) Zhang, Y.; Tang, Q.; Li, H.; Hu, W. *Appl. Phys. Lett.* **2009**, *94*, 203304. (e) Xiao, K.; Li, R.; Tao, J.; Payzant, E. A.; Ivanov, I. N.; Puretzky, A. A.; Hu, W.; Geohegan, D. B. *Adv. Funct. Mater.* **2009**, *19*, 3776–3780.
(10) (a) Bao, Z.; Lovinger, A. J.; Brown, J. *J. Am. Chem. Soc.* **1998**, *120*, 207–208. (b) Tang, Q.; Li, H.; Liu, Y.; Hu, W. *J. Am. Chem. Soc.* **2006**, *128*, 14634–14639. (c) Tang, Q.; Tong, Y.; Hu, W.; Wan, Q.; Bjørnholm, T. *Adv. Mater.* **2009**, *21*, 4234–4237.
(11) Yoon, S. M.; Song, H. J.; Hwang, I.; Kim, K. S.; Choi, H. C. *Chem. Commun.* **2010**, *46*, 231–233.
(12) (a) Kloc, C.; Simpkins, P. G.; Siegrist, T.; Laudise, A. R. *J. Cryst. Growth* **1998**, *182*, 416–427. (b) Laudise, R. A.; Kloc, C.; Simpkins, P. G.; Siegrist, T. *J. Cryst. Growth* **1998**, *187*, 449–454. (c) Briseno, A. L.; Mannsfeld, S. C. B.; Ling, M. M.; Liu, S. H.; Tseng, R. J.; Reese, C.; Roberts, M. E.; Yang, Y.; Wudl, F.; Bao, Z. N. *Nature* **2006**, *444*, 913–917.

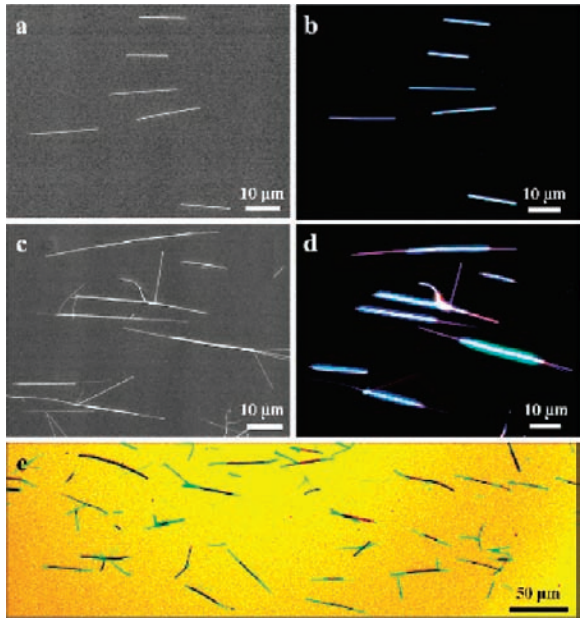

Figure 2. (a, b) SEM and dark-field optical images of CuPc nanoribbons grown on OTS-modified SiO_2 substrates. (c, d) SEM and dark-field optical images of the F_{16}CuPc nanoribbons grown on the templates of CuPc nanoribbons. (e) Large-area optical image of the p−n junction nanoribbons.

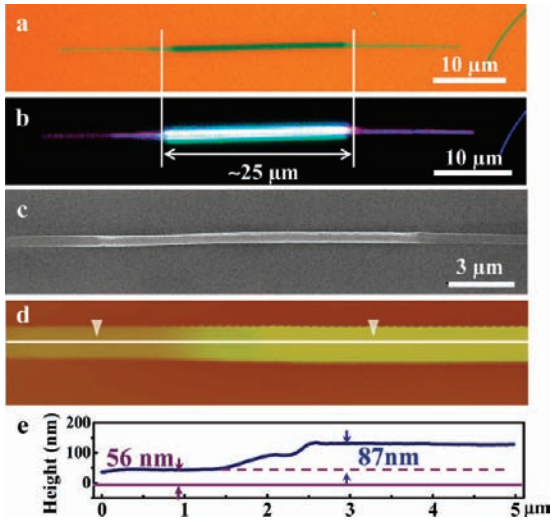

Figure 3. (a, b) Optical images of an individual p−n junction nanoribbon. (c) SEM image of an individual nanoribbon showing the p−n junction. (d) AFM image and (e) height curve of the nanoribbon, showing the distinct junction.

large-area well-ordered arrays, is of great significance in utilizing high-performance organic single-crystal devices for electronic applications.[12c] However, it is difficult to fabricate organic single-crystal p−n junctions on a large scale like those of heterostructures based on thin-film organic semiconductor materials. With this method, it may be possible to pattern organic p−n junction nanoribbons on large scales.

An individual p−n junction nanoribbon is shown in Figure 3. The active p−n junctions could be grown to lengths of ∼25 μm and unambiguously identified by optical microscopy (Figure 3b). The length of the p−n junction depends on the length of the CuPc template and the crystallization time of F_{16}CuPc on the CuPc template. An SEM image of an individual p−n nanoribbon with a length of several micrometers is shown in

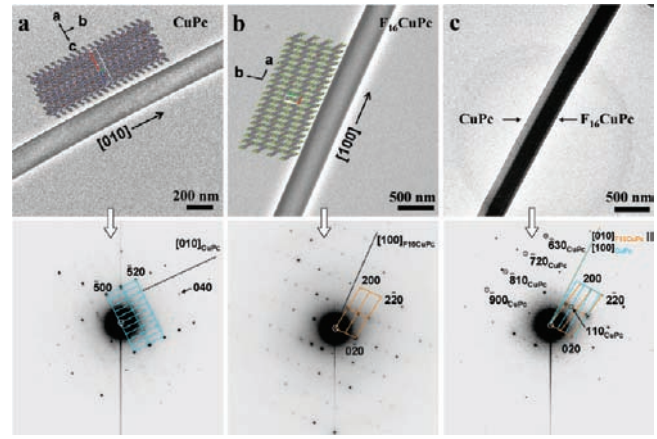

Figure 4. TEM images and corresponding SAED patterns of (a) CuPc, (b) F_{16}CuPc, and (c) p−n junction nanoribbons of CuPc and F_{16}CuPc. The insets in (a) and (b) show schematic views down the reciprocal-cell *c* axes (i.e., perpendicular to the respective *ab* planes). The SAED pattern of the p−n junction provides evidence that the two nanoribbons grow with their short principal lattice vectors (*a* axis of CuPc and *b* axis of F_{16}CuPc) matching exactly.

Figure 3c. From the AFM measurements shown in Figure 3d,e, the thickness of the p−n junction was found to be ∼143 nm, consisting of 87 nm of F_{16}CuPc and 56 nm of CuPc. Finally, Raman spectroscopy was also employed to verify the structures of the p−n junction nanoribbons (Figure S1 in the Supporting Information; for comparison, the Raman spectra of CuPc and F_{16}CuPc nanoribbons are also displayed in Figure S1). It was evident that the p−n junction nanoribbon had integrated all of the peaks of CuPc and F_{16}CuPc nanoribbons, providing direct proof of the p−n junction nanoribbons of CuPc and F_{16}CuPc.

Structural analysis of the p−n junction nanoribbons was carried out using TEM and selected-area electron diffraction (SAED) patterns. TEM images and the corresponding SAED patterns of CuPc, F_{16}CuPc, and p−n junction nanoribbons are shown in Figure 4. With the assumption that the bulk unit cell parameters of CuPc[9c] and F_{16}CuPc[10b,11] apply to the nanoribbon crystal structure, the diffraction patterns in Figure 4a,b could be identified and indexed as (001) planes of CuPc and F_{16}CuPc, respectively. The SAED pattern of the p−n junction nanoribbon contains contributions from both materials' (001) planes, which means that the interface in the F_{16}CuPc/CuPc heterocrystal is formed by the individual (001) planes. A precise analysis of the rather complicated diffraction pattern of the p−n junction is provided in Figure S2 in the Supporting Information. It was determined that the F_{16}CuPc nanoribbon grows with its (001) plane rotated in such a way that the two short principal lattice axes (i.e., the *a* axis of F_{16}CuPc and the *b* axis of CuPc) match (are identical). This situation is an interesting border case of organic−organic heteroepitaxy that would be described as *uniaxially commensurate* (i.e., the two lattices share exactly one lattice vector). In the case of epitaxial growth of spatially extended 2D crystallites on top of one another, this type of lattice matching with the substrate is not expected to provide a significant energetic benefit.[13,14] However, the situation might be different when the heterogeneous nucleation occurs on more 1D-shaped substrates such as the CuPc nanoribbons (as il-

(13) (a) Mannsfeld, S. C. B.; Leo, K.; Fritz, T. *Phys. Rev. Lett.* **2005**, *94*, 056104. (b) Mannsfeld, S. C. B.; Fritz, T. *Phys. Rev. B* **2005**, *71*, 235405. (c) Mannsfeld, S. C. B.; Fritz, T. *Phys. Rev. B* **2004**, *69*, 075416.
(14) Mannsfeld, S. C. B.; Fritz, T. *Mod. Phys. Lett. B.* **2006**, *20*, 585–605.

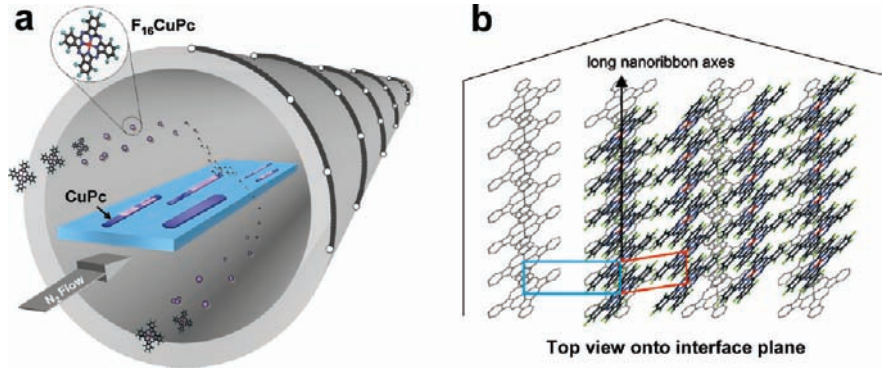

Figure 5. (a) Schematic of the physical vapor transport growth apparatus, illustrating the growth of F_{16}CuPc on CuPc nanoribbon crystals. (b) Schematic top view of the interface between the (001) planes of F_{16}CuPc and CuPc. The two molecular lattices are aligned along the matching short lattice constant (respective $\pi-\pi$ stacking axis).

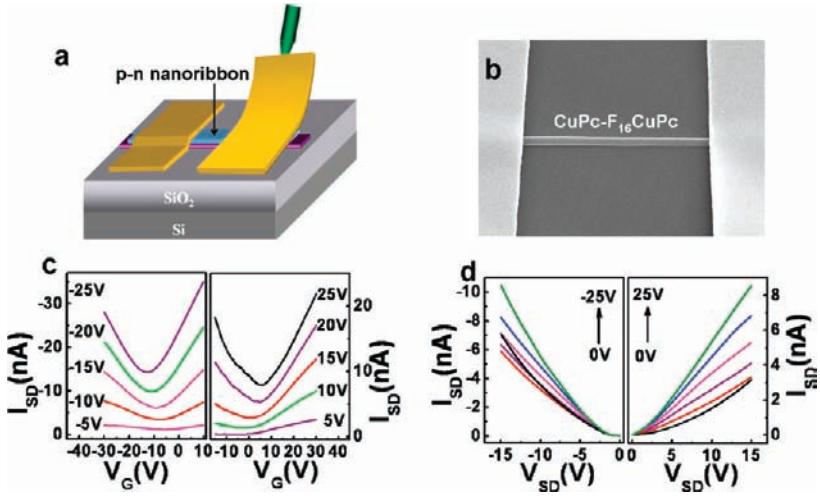

Figure 6. (a) Schematic of the fabrication of a device based on a discrete p−n nanoribbon by the "stamping electrode" technique, in which the nanoribbon was grown on a SiO_2 substrate and gold source and drain electrodes were placed on the nanoribbon. (b) SEM image of an individual p−n junction transistor. (c) Transfer and (d) output characteristics of an ambipolar p−n transistor.

lustrated in Figure 5a). One could imagine that the nucleation of F_{16}CuPc starts with rows of F_{16}CuPc molecules stacked in the principal $\pi-\pi$ stacking direction (along the *a* axis) (see Figure 5b). Such a row can naturally and thus rapidly extend along the *b* axis of the underlying (001) surface of CuPc because on that surface, the best binding site for F_{16}CuPc repeats with a periodicity that is also native to the [100] stacks of the F_{16}CuPc bulk crystal (with a negligible mismatch of ∼0.13%). As long as the rate of nucleation is low (as it is in PVT),[15] such a row can grow into a single-crystalline nanoribbon.

The single-crystalline nature of the p−n junction nanoribbons indicates their high quality and potential use in devices and circuits. As an example, organic field-effect transistors of discrete p−n junction nanoribbons were fabricated and tested. All of the nanoribbons were grown in situ on the substrates by PVT[16] to avoid surface contamination and damage of the crystals during the mechanical transfer process for device fabrication and allow an intimate contact between the nanoribbon and the octadecyltrichlorosilane (OTS)-modified SiO_2 substrate to be established. The OTS-modified surface greatly improved the performance of the devices relative to those grown on bare Si/SiO_2 substrates. This is likely due to the decrease of traps at the semiconductor/dielectric interface. Gold source and drain electrodes were fabricated on single-crystal nanoribbons by the "stamping technique".[17] A schematic diagram and representative SEM image for the device fabricated using this technique are shown in Figure 6. The transfer characteristics of the p−n junction nanoribbon device measured in air and at room temperature are shown in Figure 6c. From the transfer characteristics in Figure 6c, the effective field-effect mobilities (μ) of CuPc and F_{16}CuPc transistors were calculated as 0.07 and 0.05 $cm^2\ V^{-1}\ s^{-1}$, respectively. The performances of the transistors were highly stable and reproducible in air, indicating the environmental stability of both the p- and n-type transistors. The devices exhibited a typical "V-shape" characteristic, wherein one arm was for electron transport and the other was for hole transport, confirming the ambipolar behavior of the transistors. The balanced hole and electron transport were assigned to the hole and electron mobility of the single-crystalline nanoribbons of CuPc and F_{16}CuPc, which is very important in double-carrier devices, such as complementary digital circuits and solar cells.

As a final demonstration of their p−n nature, we fabricated a discrete p−n junction nanoribbon photovoltaic solar cell.

(15) Mannsfeld, S. C. B.; Briseno, A. L.; Liu, S.; Reese, C.; Roberts, M. E.; Bao, Z. *Adv. Funct. Mater.* **2007**, *17*, 3545–3553.
(16) Tang, Q.; Li, H.; Song, Y.; Xu, W.; Hu, W.; Jiang, L.; Liu, Y.; Wang, X.; Zhu, D. *Adv. Mater.* **2006**, *18*, 3010–3014.
(17) Tang, Q.; Tong, Y.; Li, H.; Ji, Z.; Li, L.; Hu, W.; Liu, Y.; Zhu, D. *Adv. Mater.* **2008**, *20*, 1511–1515.

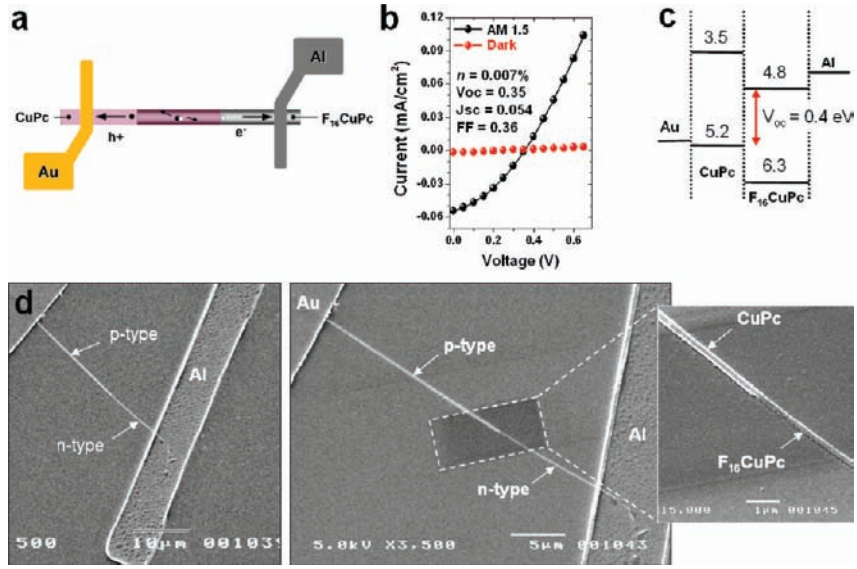

Figure 7. (a) Schematic configuration of a discrete p−n junction solar cell, showing how holes and electrons are separated and transported at the CuPc−F_{16}CuPc interface. (b) Current−voltage characteristics showing ideal photocurrent. (c) Band diagram showing a "theoretical" open-circuit voltage of 0.4 eV (similar to the experimental value of 0.35 eV). (d) SEM image of a discrete CuPc−F_{16}CuPc nanoribbon photovoltaic solar cell. The estimated AM 1.5 G efficiency of the device was based on the projected active area (length × width) of the p−n nanoribbon.

Figure 7a shows a schematic configuration of a p−n device, while Figure 7b shows the current−voltage (I−V) characteristics for the device whose SEM image is shown in Figure 7d. The plot for a CuPc−F_{16}CuPc nanoribbon device yielded a short-circuit current density (J_{SC}) of ∼0.054 mA/cm^2, an open-circuit voltage (V_{OC}) of ∼0.35 V, a fill factor (FF) of ∼0.36, and an efficiency (η) of ∼0.007% under 1 sun (100 mW/cm^2). Although our devices showed low efficiencies, our conclusion from these first measurements is that discrete p−n nanoribbon devices will allow more precise control over and characterization of the properties, thus significantly reducing the uncertainty in data interpretation in comparison with polycrystalline bilayer devices. The p−n nanoribbons will also serve as ideal systems for understanding the fundamental charge-transport and photovoltaic behaviors at nanoscale organic−organic interfaces (Figure 7a). Ongoing work will include optimizing the choice of metal contacts and improving our fabrication techniques to extract more efficient parameters. We are also extending this method of crystallization to other semiconductors that exhibit a larger separation between the valence and conduction bands of the respective p- and n-type materials.

Conclusion

In summary, organic single-crystalline p−n junction nanoribbons of CuPc and F_{16}CuPc were synthesized on a large scale by crystallization of F_{16}CuPc on CuPc nanoribbon templates. The selective crystallization strongly depended on the similar molecular structures and lattice parameters at the interfacial basal planes of the (001) facets of F_{16}CuPc and CuPc. Well-defined ambipolar transport characteristics with balanced mobilities were demonstrated on discrete devices, indicating their suitability for use in solar cells and complementary circuits. Solar cells fabricated from individual p−n nanoribbons demonstrated photocurrent rectification when irradiated at AM 1.5, thus showing great promise for studying photoinduced charge transport at organic−organic interfaces. This work opens the door to opportunities for exploring the synthesis of high-quality organic single-crystalline p−n junction nanoribbons and their application in fundamental science and new device technologies.

Acknowledgment. A.L.B. acknowledges partial support by the NSF Materials Research Science and Engineering Center on Polymers at UMass Amherst (DMR-0820506) and the Center for Hierarchal Manufacturing (CMMI-0531171). W.H. acknowledges financial support from National Natural Science Foundation of China (20721061, 20872146, 50725311, 60801037), the China−Denmark Coproject, TRR61 (NSFC−DFG Transregio Project), the Ministry of Science and Technology of China (2006CB806200, 2006CB932100, 2009CB930400), and the Chinese Academy of Sciences.

Supporting Information Available: Experimental details, Raman spectra of p−n nanoribbons, and detailed analysis of the SAED characterization data. This material is available free of charge via the Internet at http://pubs.acs.org.

JA102779X